

CHARACTERIZATION OF A 2-D POOL FIRE SIMULATOR[†]

Peter J. Disimile

USAF 46 Test Wing, Aerospace Survivability and Safety Flight
Wright-Patterson AFB, Ohio 45433-7605, USA
peter.disimile@wpafb.af.mil
937-255-6823 ext. 212

John M. Davis

Engineering and Scientific Innovations Inc.
Batesville, IN 47006
jdavis@esi-solutionsinc.com
812-934-2538

ABSTRACT

The current paper introduces a facility to be used for the investigation of fire suppressant transport and pool fire extinction in an environment similar to an aircraft engine nacelle. This work is done as part of an ongoing effort to develop a suppressant transport model that could be used within the computational fire code currently under development by Sandia National Laboratory. The flow in this facility was conditioned to match airflow characteristics of typical aircraft engine nacelles and characterized using constant temperature anemometry and flow visualization. The mean streamwise velocity was found to be 6.30 m/s (20.7 ft/s) +/-10% with a nominal turbulent intensity of 5.0 % +/-1%. Flow visualization indicates the presence of a recirculation region extending upstream from the pool leading edge as well as flow being transported from the pool leading edge upstream over the clutter. This characterization will provide baseline documentation for future investigations.

INTRODUCTION

Aircraft engine nacelles present a difficult region for fire protection. Airflow in engine nacelles is commonly characterized by high turbulence levels and air exchange rates.¹ Furthermore, engine nacelles are typically highly cluttered with fuel lines and other plumbing, electric wiring bundles, structural components, etc. Figure 1 shows an example of the cluttered nacelle environment of a generic aircraft engine.

[†] This research is part of the Department of Defense's Next Generation Fire Suppression Technology Program, funded by the DoD Strategic Environmental Research and Development Program

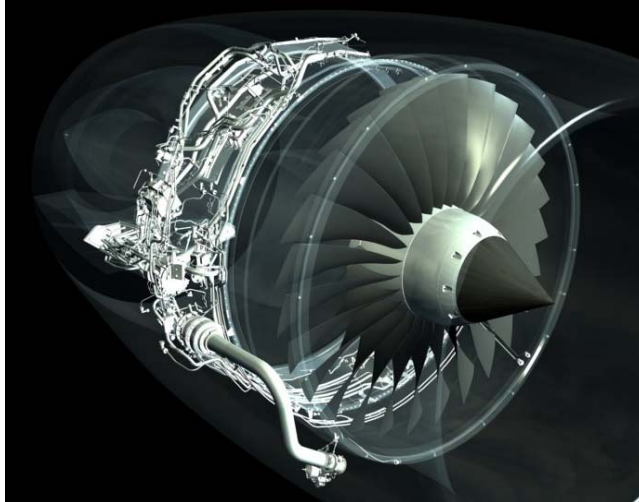


Figure 1. Generic Aircraft Engine Nacelle with Clutter.

A production ban on halogenated fire suppressants in the early 1990s adds further difficulty to the fire protection in engine nacelles. Halogenated agents were used as the main source of fire protection in engine nacelles up to the production ban. These agents were very efficient (measured by weight and/or volume) in fire suppression compared to new potential halon replacement agents.² Due to the relatively high fire suppression efficiency of halon agents, little research was conducted to investigate suppressant transport phenomena. The current paper is done as part of an ongoing effort to develop a fire suppressant transport model to better understand fire suppressant processes, as well as to be incorporated within the computational fire code currently under development by Sandia National Laboratory.

FACILITY OVERVIEW

An overall schematic of the presented facility can be seen in Figure 2. The open loop facility works in a blowing arrangement with a centrifugal blower having a maximum output of 6000 scfm installed upstream of the test section. A wide angle inlet diffuser is installed downstream of the blower via transition piece as shown in Figure 2. The inlet diffuser consists of multiple sections connected by the flanges shown in Figure 2. This enabled flow conditioning honeycomb/screens to be installed at various stages of the inlet diffuser to achieve the highest level of uniformity in the test section.

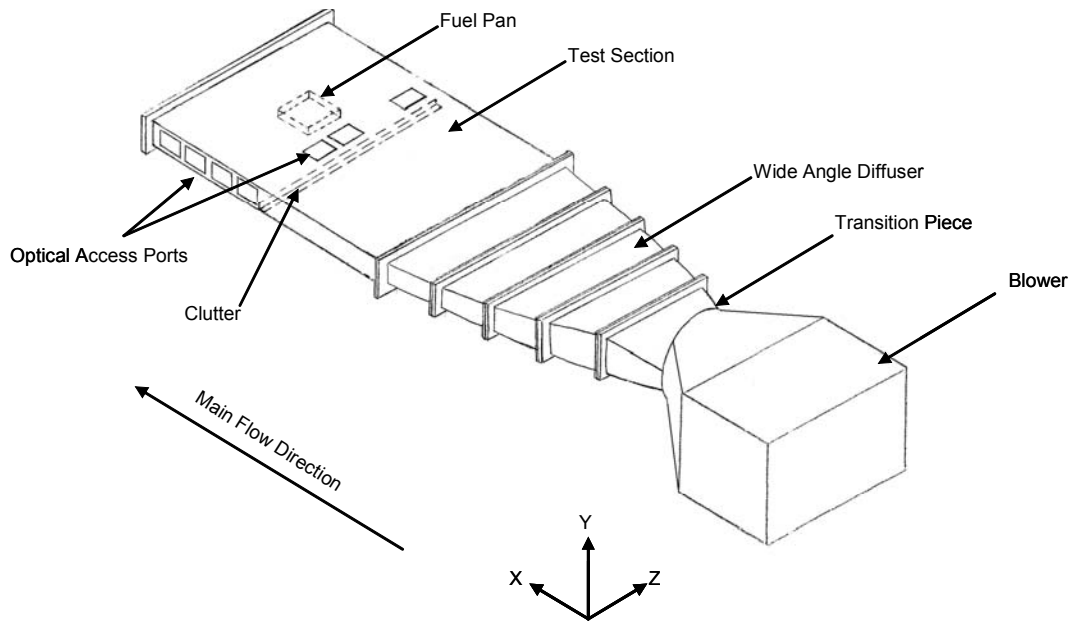


Figure 2. Facility Schematic.

Figure 3 is a close up view of the exterior of the test section looking upstream. It can be seen that the test section is 2438 mm (96.0") in length, 1829 mm (72.0") in width, and 229 mm (9.0") in height, all measured internally. Seven 165 mm x 203 mm (6.5" x 8.0") optical access ports were installed, four on the test section wall and three across the test section ceiling. The side ports were installed directly downstream of the clutter position (described below) with 58 mm (2.3") spacing, allowing a viewing area from the clutter edge downstream past the liquid pool. The three top ports were asymmetrically placed about the z-axis centerline to allow maximum access of the test section from the ceiling under the assumption of a symmetrical internal flow.



Figure 3. Test Section Overview.

Currently, the interior of the test section consists of a single perpendicular clutter element, two streamwise fences and a rectangular cavity that will serve as a liquid fuel pan, all of which can be seen in Figure 4. The clutter and fences are removable features which allow testing of the effects of flow dimensionality. The clutter element is made of 51 mm x 51 mm x 6 mm (thickness) (2.0" x 2.0" x 0.3") upstream facing angle iron and spans the entire width of the test

section. The vertical edge of this clutter element is located 1219 mm (48.0”) downstream of the test section inlet.

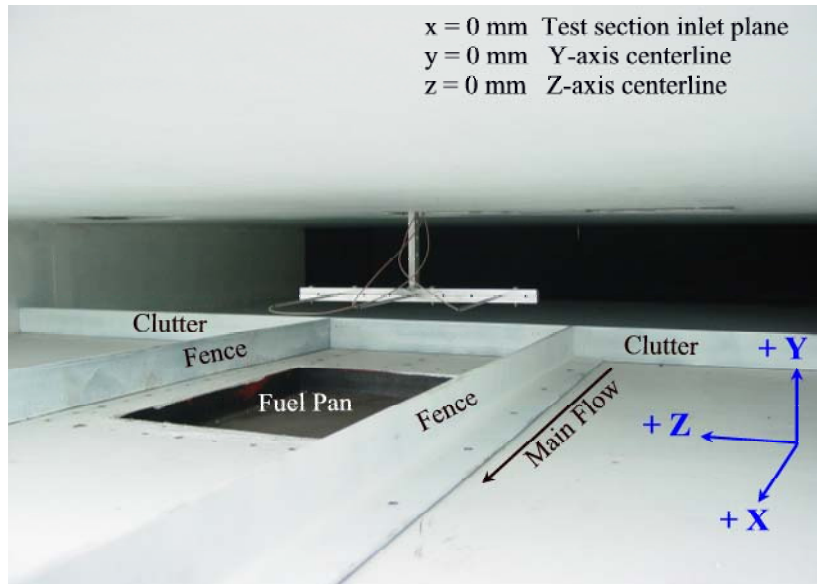


Figure 4. Test Section Internal Dimensions.

Streamwise fences flank a liquid fuel pan by 73 mm (2.9”). The fences are made of 51 mm x 51 mm x 5 mm (thickness) (2.0” x 2.0” x 0.2”) outward facing angle iron. The fences are installed directly downstream of the vertical edge of the clutter element and run the entire remaining test section length 997 mm (39.3”), see Figure 4.

A 265 mm x 384 mm (10.4” x 15.1”) liquid fuel pan is located 1441 mm (56.7”) downstream of the test section inlet which corresponds to a distance of 222 mm (8.7”) downstream of the vertical edge of the clutter element. The center of the fuel pan is located on the test section z-axis centerline.

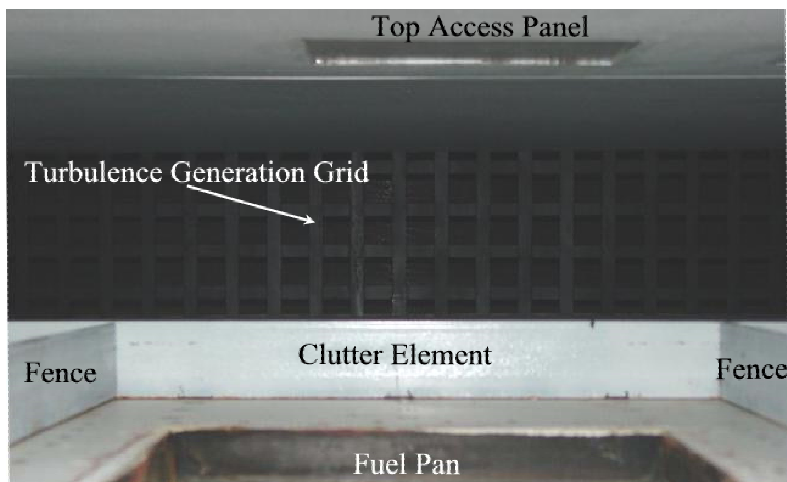


Figure 5. Turbulence Generation Grid Installed.

To provide a level of turbulence that is expected to replicate levels found in aircraft engine nacelles a turbulence generation grid was fabricated and installed at the inlet plane of the test

section. The grid utilized can be seen installed in the test section in Figure 5. The grid covers the entire cross sectional area of the test section and is made of 19 mm (0.7") wide, 3 mm (0.1") sharp edged steel flat stock arranged in a checkerboard pattern with a nominal open cell size of 38 mm x 38 mm (1.5" x 1.5").

CTA FLOW CHARACTERIZATION

Constant Temperature Anemometry (CTA) was used to characterize the flow field directly behind the clutter element. Streamwise velocity traverses were acquired at seven vertical planes across the test section width at 1230 mm (48.4") downstream of the test section inlet (11 mm downstream of the clutter). The seven z-axis locations investigated included, -478, -225, -121, 8, 136, 430, and 681 mm (-18.8", -8.9", -4.8", 0.3", 5.4", 16.9", and 26.8") measured from the centerline of the test section. From these time series the mean velocity and turbulent intensity (T.I.) were determined and the streamwise uniformity of the flow across the test section height examined at each individual z-axis location. By comparison of all seven vertical profiles the flow uniformity across the test section width can also be examined.

The set of seven velocity and T.I. profiles were determined for several test section configurations, three of which are presented herein. The clutter element described in the Facility Overview Section was installed for all configurations. The first configuration (Configuration 1) provided a baseline and consisted of the perpendicular clutter only without the streamwise fences or turbulence generation grid installed. The second configuration (Configuration 2) was used to examine the effects of the turbulence generation grid and therefore the turbulence generation grid was positioned 1219 mm (48.0") upstream of the clutter element vertical edge. The streamwise fences were installed along with the turbulence generation grid for the final configuration (Configuration 3). These three configurations are typical configurations to be used in future fire testing. Velocity and T.I. profiles for each of the three configurations follow in their corresponding subsection.

CONFIGURATION 1: NO GRID, NO FENCES

The streamwise velocity and T.I. profiles for Configuration 1 are presented in Figure 6 and Figure 7, respectively. The edge of the clutter and the test section floor are depicted by the solid grey and black lines, respectively. Data was acquired at y-axis locations ranging from -90.49 mm to 87.31 mm (-3.56" – 3.44") with an increment of 6.35 mm (0.25"), thereby examining the flow in the center region 25.00 mm (1.00") from the upper and lower test section walls.

It can be seen in Figure 6 that the flow directly behind the clutter (data points between the solid grey and black lines) has a relatively low velocity compared to the velocity at the center. This is expected since the flow cannot follow the sharp turn caused by the vertical clutter and therefore will separate, causing a recirculation region directly behind the clutter. Since CTA is not capable of detecting flow reversals, the accuracy of the data measured in this region cannot be validated, however, it does show evidence of flow separation. The extent of this recirculation region was determined using flow visualization (discussed below).

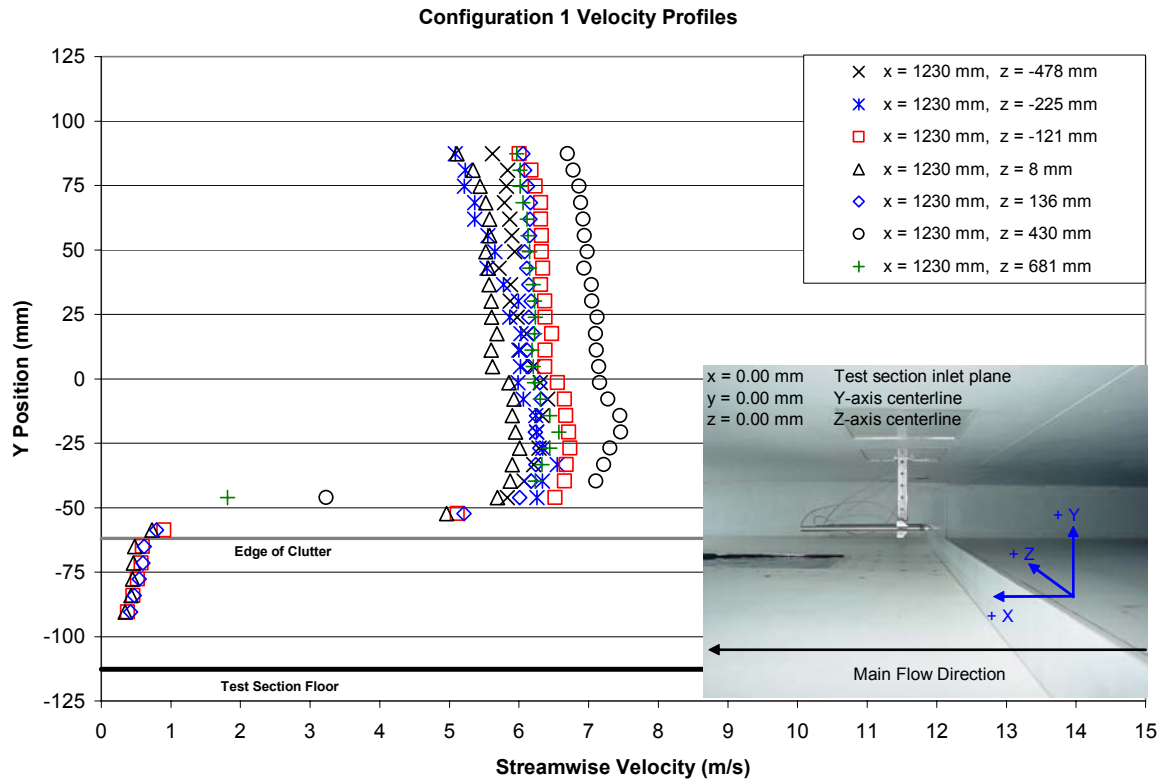


Figure 6. Velocity Profiles: No Grid, No Fence.

Directly above the clutter edge (between -60 mm to -50 mm) the velocity drastically increases from approximately 1 m/s to 6.5 m/s. In the region between -50 mm and -25 mm, an overshoot in the velocity profiles is evident, which is a typical effect found in contracting flows, sometimes referred to as a dog ear. The edge of the shear layer can be clearly seen (Figure 7) to be located at approximately -25 mm, where a sudden change in the T.I. profile is evident. Above the -25 mm position, the turbulence intensity remains relatively constant at approximately 1%. Below the -25 mm position, the T.I. increases to approximately 13% at the upper edge of the clutter. Just below the upper edge of the clutter the T.I. level increases further to approximately 15%, however, these locations are in the recirculation region that exists downstream of the clutter.

Each of the seven velocity profiles follow a similar trend with the lowest velocity measured toward the test section ceiling (y position of approximately 87 mm) and the maximum velocity measured at approximately y = -25mm. The flow uniformity across the test section height can be addressed by examination of each of the seven velocity and T.I. profiles individually. The velocity profiles at each z-axis location show a uniformity of up to +/- 7%, while the uniformity of the T.I. is within a maximum of +/-0.5% with the exception of z-axis locations of -478 and -225 mm at which the T.I. profiles deviated by up to +/-1%.

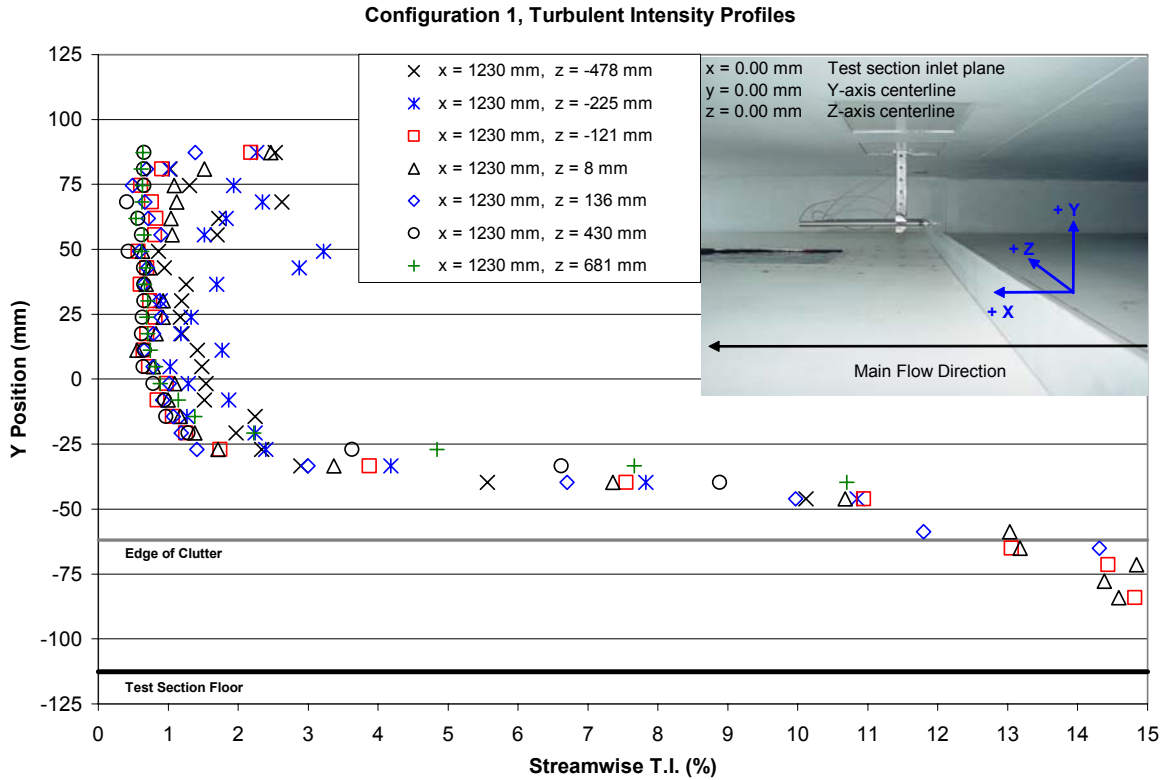


Figure 7. T.I. Profiles: No Grid, No Fences.

Flow uniformity across the test section width can be calculated by comparing the seven widths examined for one y-position. The upper and lower velocity extremes were measured at z-axis locations of 8 and 430 mm. The velocity between these two z-axis profiles deviated by +/-10% across the test section height. The T.I. profiles are all in close agreement with the exception of the -478 and -225 mm z-axis locations which deviated by up to 2% from the other five z-axis locations examined.

CONFIGURATION 2: WITH GRID, NO FENCES

The measurements described above for the Configuration 1 were repeated for Configuration 2. Measurement locations below $y = -50$ mm were omitted since they offered little insight into the flow uniformity as determined from the profiles shown above for Configuration 1. The resulting velocity and T.I. profiles for Configuration 2 are presented in Figure 8 and Figure 9, respectively.

From comparison of Figure 8 and Figure 6, it can be seen that the turbulence generation grid increased the uniformity across the test section width. A linear fit of the data shown in Figure 8 (not shown) yielded an average velocity of 6.6 m/s +/- 10%.

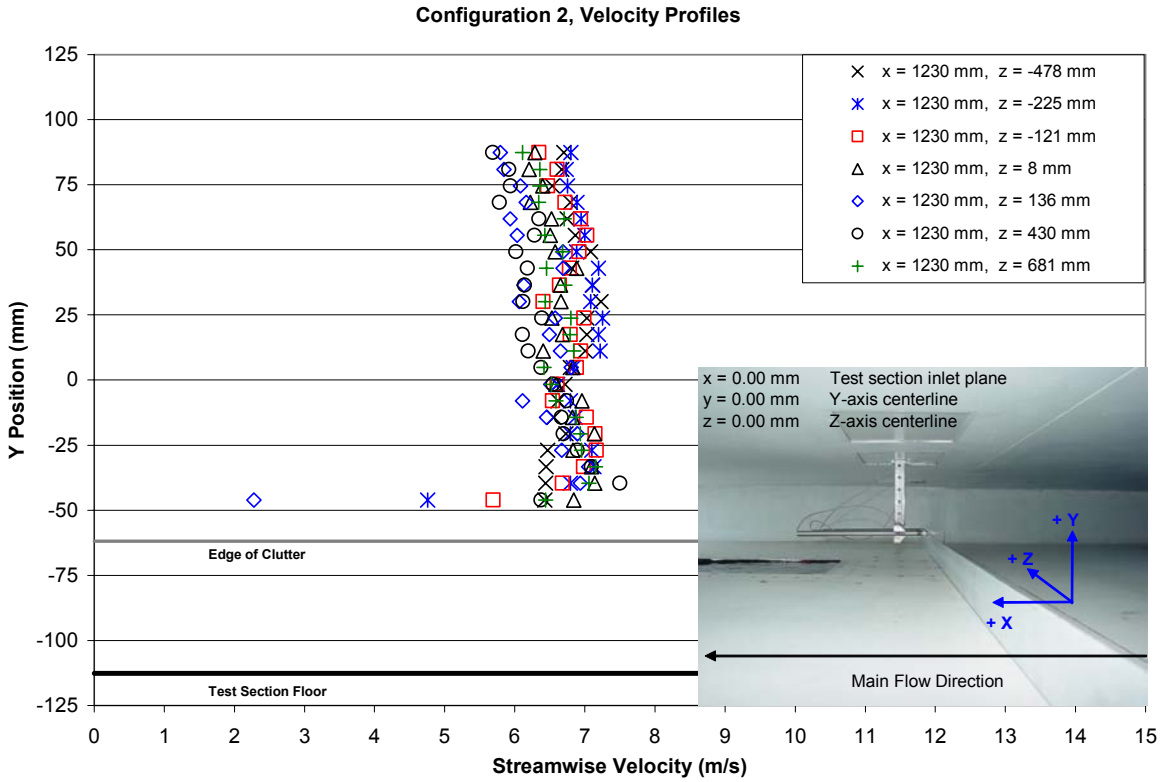


Figure 8: Velocity Profiles: With Grid, No Fences

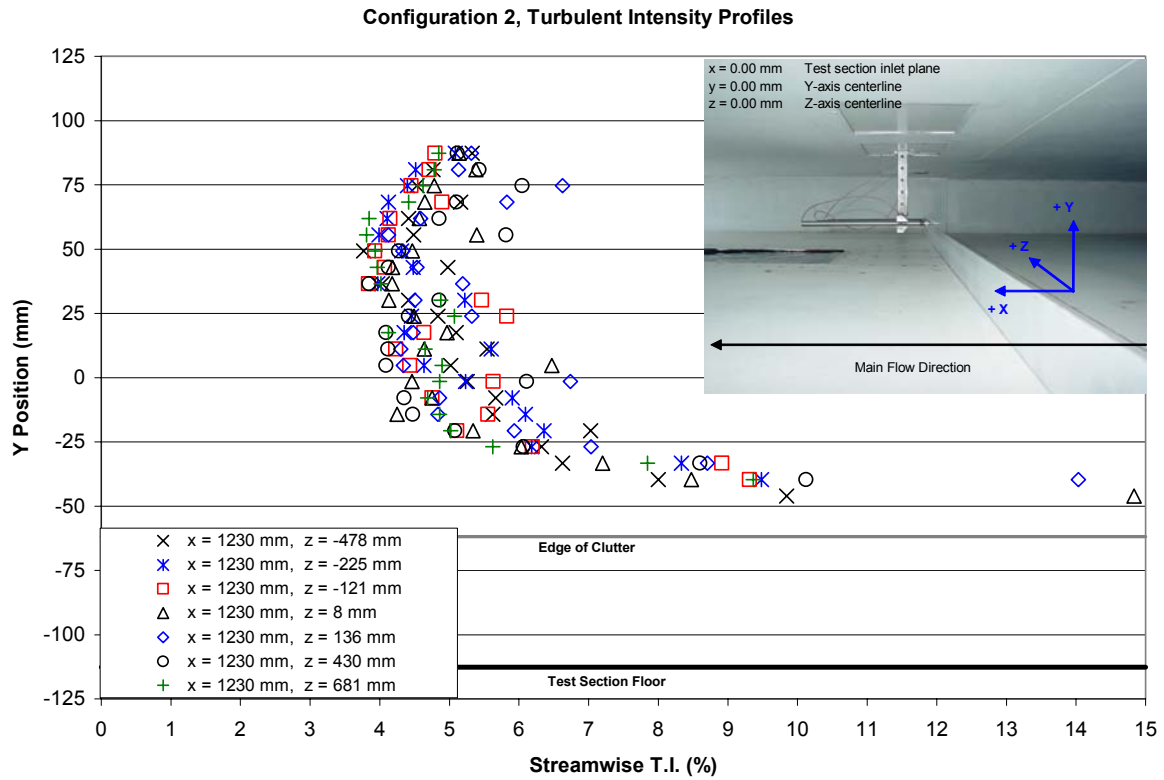


Figure 9: T.I. Profiles: With Grid, No Fences

The effect of the turbulence generation grid on the test section airflow turbulence level can be seen by comparing Figure 9 and Figure 7. Overall the T.I. profiles have shifted to approximately the 5% level with the turbulence generation grid installed. A drastic increase in the T.I. around $y = -25$ mm indicates that the shear layer edge is located in approximately the same location as described above for Configuration 1. Also, it is evident that the turbulence generation grid decreased the y-axis uniformity in the T.I. profiles, however, this slight negative effect is outweighed by an increase in T.I. to acceptable levels for simulation of nacelle conditions and an increase in the velocity profile uniformity. An overall fit of the T.I. profiles (not shown) yielded an average T.I. of approximately 5% with a $\pm 1.5\%$ agreement across the test section.

CONFIGURATION 3: WITH GRID, WITH FENCES

The measurements described above for Configuration 2 were again repeated for Configuration 3, to study the effect of the streamwise fences. Figure 10 and Figure 11 are the resulting velocity and T.I. profiles for Configuration 3, respectively. A linear fit of the profiles yielded an average velocity and T.I. in this configuration of 6.3 m/s $\pm 7\%$ and approximately 5% $\pm 1\%$, respectively.

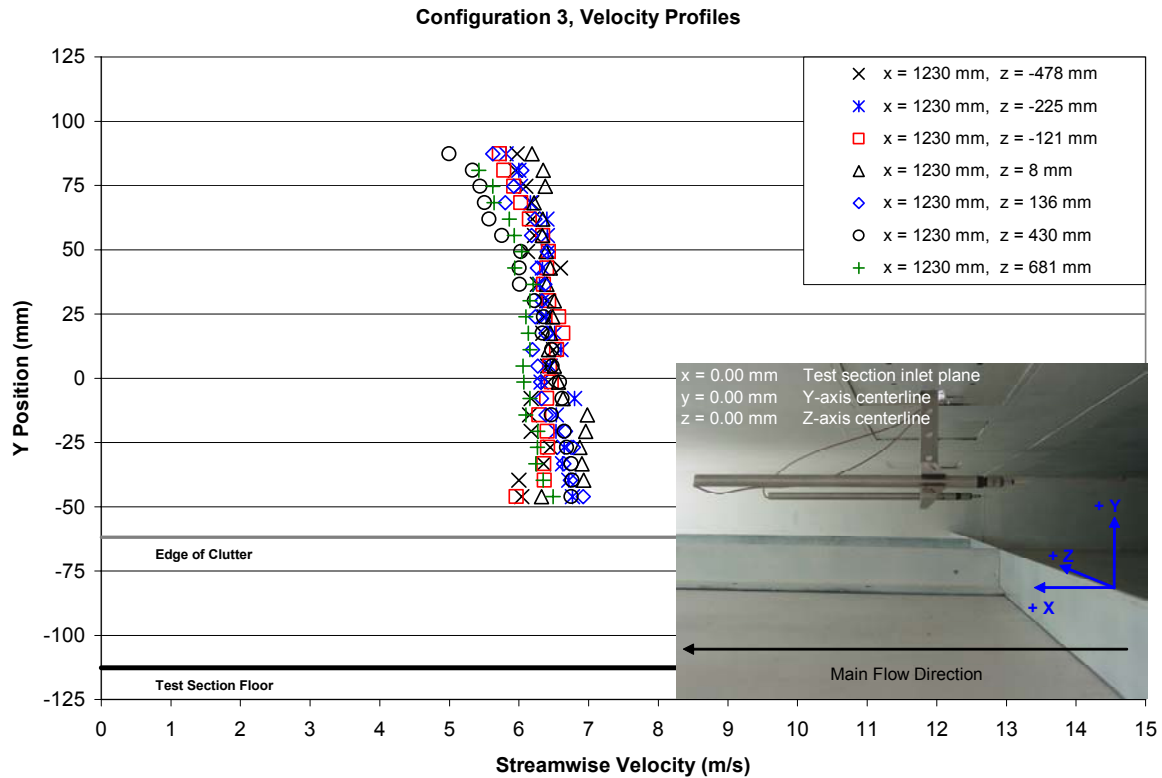


Figure 10. Velocity Profiles: With Grid, With Fences.

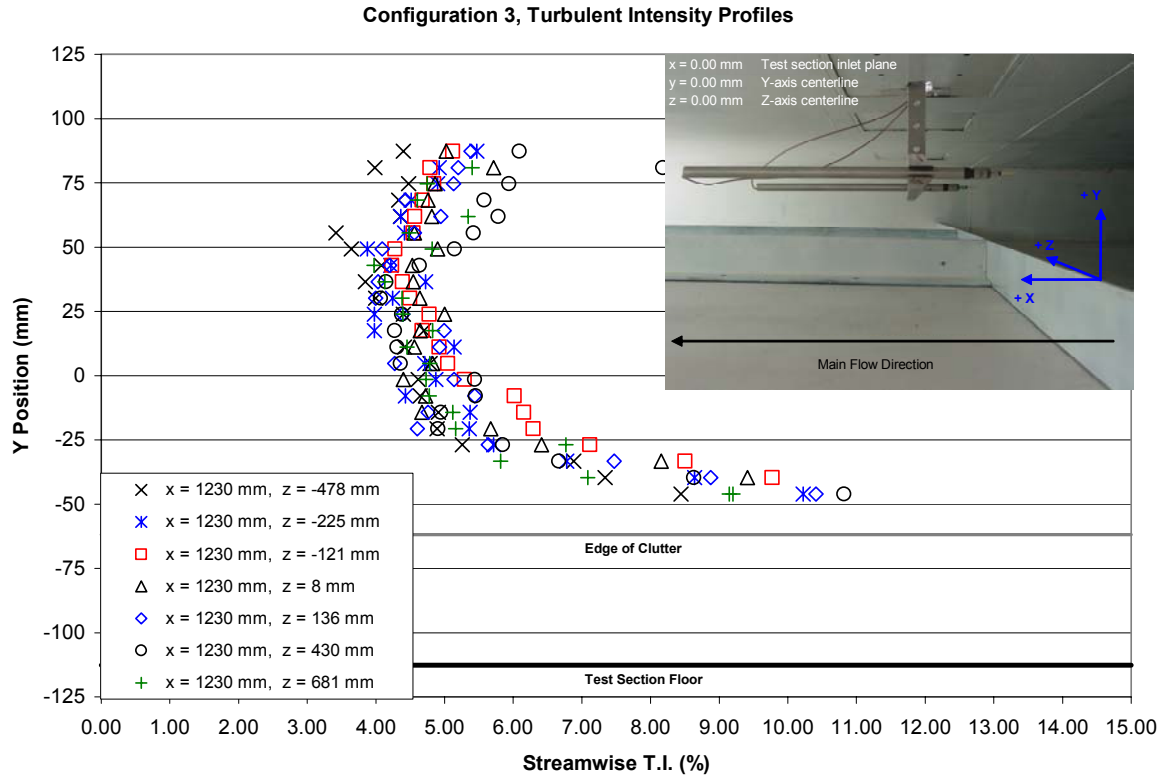


Figure 11: T.I. Profiles: With Grid, With Fences

FLOW VISUALIZATION

Flow visualization was conducted to determine the boundaries of the recirculation region that exist directly downstream of the perpendicular clutter. Characterizing the recirculation region (whether qualitatively or quantitatively) is of importance since preliminary computational results have shown the possibility of flame propagation upstream from the fuel pan leading edge to the perpendicular clutter element. If the recirculation region downstream of the clutter extends down to or beyond the leading edge of the fuel pan, the upstream propagation of a flame is possible.

The flow was visualized using smoke produced from incense sticks attached to the test section floor. Illumination was provided using a 500 watt halogen light oriented vertically perpendicular to the viewing plane. Initial flow visualization video was recorded using a standard frame rate (30 fps) SVHS camera set to a shutter speed of 1/1000 second. Follow up testing was recorded using a high speed CMOS digital camera operating at the same shutter speed. Images were recorded at 120 frames per second for follow up testing. Flow visualization experiments were conducted for both steady state and tunnel startup conditions for Configuration 2 only.

A video sequence of 16 frames representing the tunnel startup condition is shown in Figure 12. The time between each frame is 33 ms. The incense sticks were positioned on the test section floor 13 mm (0.5”) downstream of the clutter element on the z-axis centerline. The first frame (upper left corner of Figure 12) depicts the tunnel just after startup. The smoke stream prior to tunnel start was vertical.

With the first two frames in Figure 12 we see that the smoke stream is bent downstream by the oncoming airflow. However, rather than completely displaced downstream, the smoke adjacent to the test section floor is drawn upstream. This can be seen by observing frames 5-6. In frame 6 the smoke initially drawn upstream is beginning to be entrained into the shear layer produced by the clutter element. Further smoke entrainment into the shear layer and visual formation of the nascent vortical structures becomes evident by frame 7.

Rollup of these small vortical structures are further developed in frame 8, at which point the small vortices begin to roll into a larger vortical structure which represents the recirculation region downstream of the clutter. From frame 8 on, the smaller vortices combine and continue to rotate into a large vortical structure which begins to stretch and extend downstream from the edge of the clutter element. As the smoke traces rotate and become more mixed with surrounding air the contrast is reduced and therefore the flow details become harder to visualize. This sequence shows the initial start and growth of the recirculation region located downstream of the clutter element.

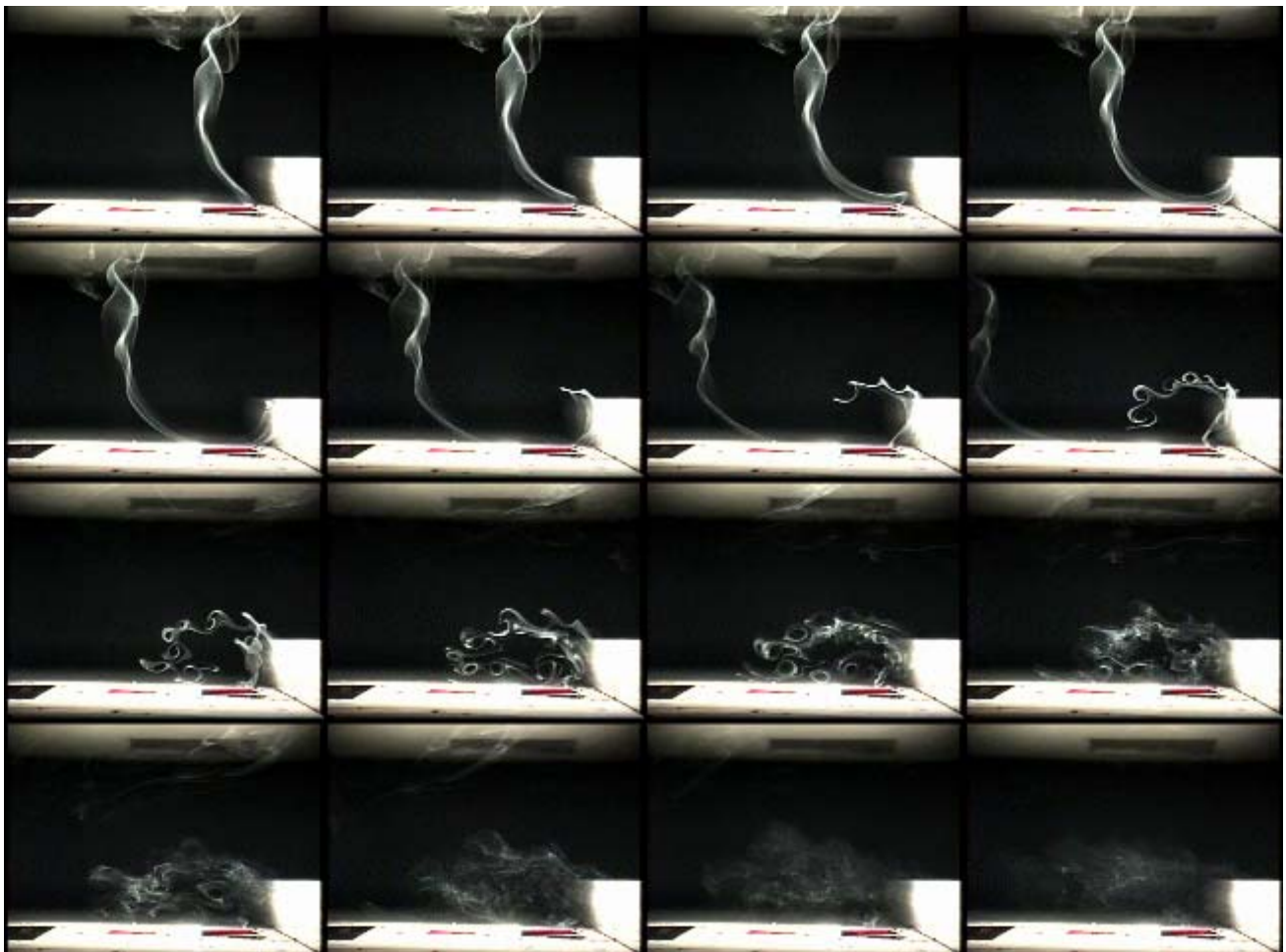


Figure 12. Startup Vortex Smoke Visualization Sequence.

Qualitatively, the images in Figure 12 help explain the recirculation region development. However, quantitative results can be resolved from Figure 12 by observing in the last few frames

that the recirculation region has extended to approximately 170 mm (~6.8") downstream of the clutter, approximately 52 mm (2.0") upstream of the pan leading edge. Further growth of the recirculation region is possible, however, cannot be depicted in the current smoke visualization studies due to high mixing and dissipation of the concentrated smoke lines.

In an attempt to locate the downstream edge of the recirculation region several incense sticks were placed at four locations downstream of the clutter edge. These locations included 25 mm (1.0"), 76 mm (3.0"), 127 mm (5.0") downstream of the clutter edge and on the leading edge of the fuel pan. At tunnel startup, the video appeared similar to that shown in Figure 12, except that the two furthest downstream smoke trails appeared to be immediately blown downstream. However, at steady state the recirculation region effect can still be seen. A sequence of 9 consecutive frames (33 ms frames rate) during steady state tunnel operation can be seen in Figure 13. During a run, a piece of ash shed from the incense located at the fuel pan leading edge was observed. This can be seen in frame 3 of Figure 13. Following this ash (encircled in red) to frame 4, 5, 6 and 7 shows upstream motion of this particle to a point (frame 7) where it becomes deeply entrained into the shear layer and is transported downstream. This confirms that flow closer to the floor is moving upstream from the fuel pan leading edge, hence the recirculation region downstream of the clutter must extend at least to the fuel pan leading edge.

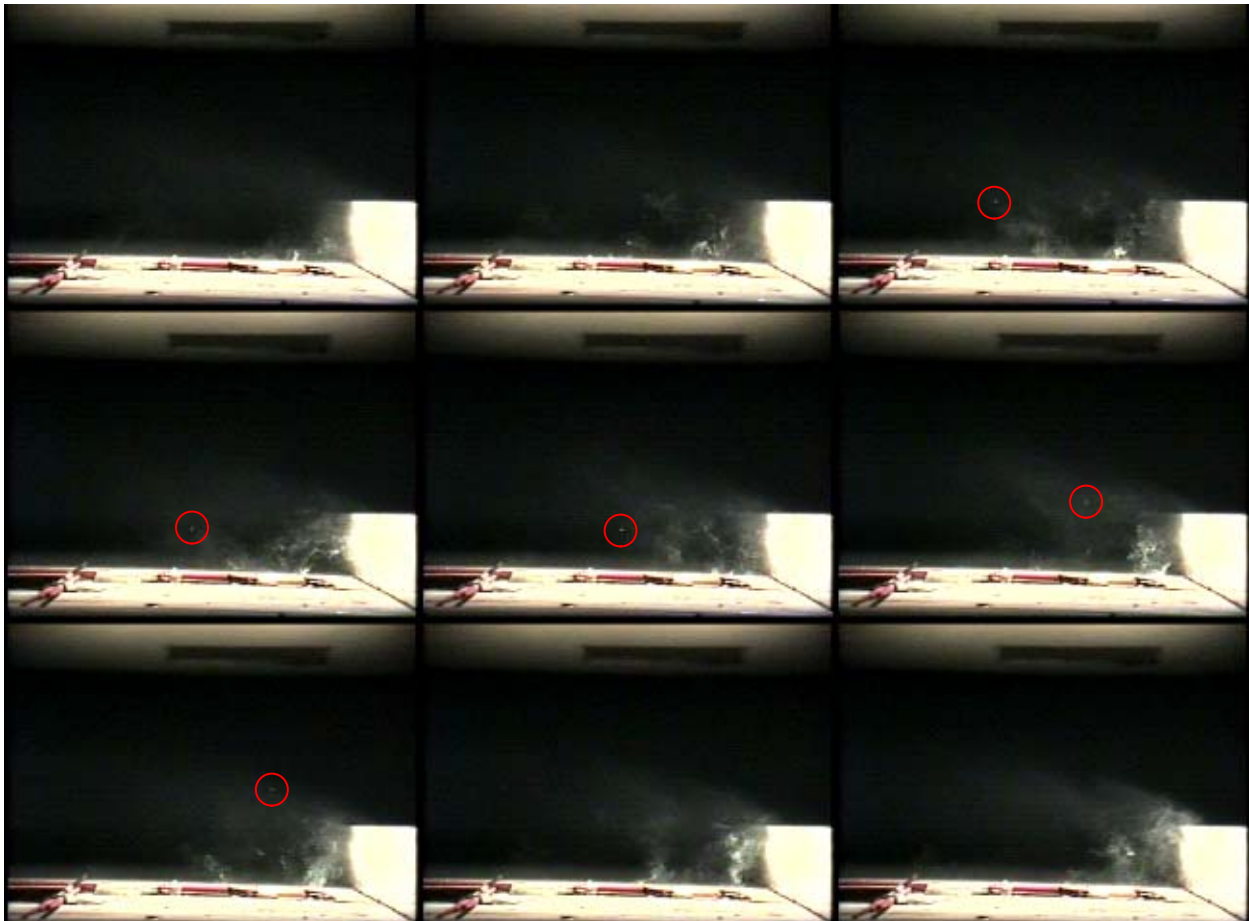


Figure 13. Steady-State Smoke Visualization Sequence.

A larger still image (Figure 14) taken from the same run shown in Figure 13 provides further support that the recirculation region is extending to the leading edge of the fuel pan. Also of importance in Figure 14 is the quantity of smoke that has propagated upstream over the vertical edge of the clutter element. Since no smoke was introduced upstream of the clutter, the smoke observed in this picture must have originated downstream of the clutter and was drawn upstream by a smaller recirculation region existing directly upstream of the clutter element. Such a region, similar to the situation of flow over a forward facing step, is expected. If this smaller recirculation region was viewed from the side the flow would be circulating in a counterclockwise direction. The circulation of the flow downstream of the clutter has been shown to also rotate in a counterclockwise direction. Thus directly upstream of the clutter the flow experiences a downward motion, while directly downstream of the clutter the flow will experience an upward motion. Since the shear layer is detached from the clutter vertical edge, the smoke/flow adjacent to the clutter edge in the downstream recirculation region is entrained by the smaller upstream recirculation region. The evidence of smoke upstream of the clutter in Figure 14 confirms this condition.

Lastly, Figure 14 can be used to find the approximate thickness of the shear layer. Using scaling (i.e. the clutter is 51 mm), it was determined that the shear layer is approximately 25 mm (1.0") thick at the edge of the clutter. This supports the approximate location of the shear layer edge determined by examination of the velocity and T.I. profiles.

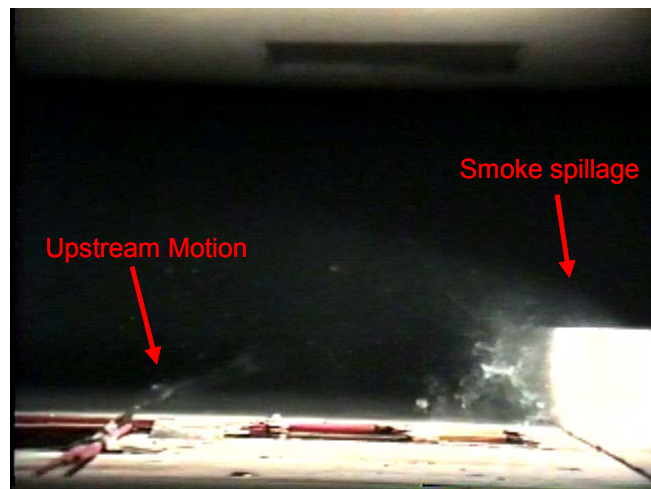


Figure 14. Steady-State Smoke Visualization.

Further flow visualization was conducted by placing incense sticks both upstream and downstream of the clutter at various locations. The incense sticks were separately placed in distinct locations yielding individual movies for each location examined. These movies were precisely timed upon tunnel startup which allowed them to be superimposed onto one another. A sequence of 9 frames (67 ms between frames) of a composite video taken during tunnel startup condition is shown in Figure 15.

The sequence shown in Figure 15 contains seven superimposed videos which correspond to seven initial locations of the incense sticks. Each smoke stream was artificially colored (using video editing software) to provide separation between the smoke streams. The seven locations

are best described by their corresponding color in Figure 15. The orange stream is initially located on the upstream lip of the forward clutter element (lip between the test section floor and the horizontal leg of the angle-iron). The teal smoke stream originates from the upstream corner of the clutter element (inside corner of the angle-iron). The purple smoke stream originates from incense placed on the top of the vertical edge of the clutter element while the green smoke is initially located directly downstream of the vertical edge of the clutter on the test section floor. The red, yellow, and blue smoke streams originate from 25 mm (1.0"), 64 mm (2.5"), and 95 mm (3.8") downstream of the clutter edge.

The seven separate smoke streams can easily be seen just after tunnel start in the first frame of Figure 15. It should be emphasized that Figure 15 is a composite video of seven superimposed separate test runs, thus the interactions between the flow details are not justified. However, the timing is correct, and Figure 15 provides a good way to visualize how smoke from several locations propagates over the clutter upon tunnel startup.

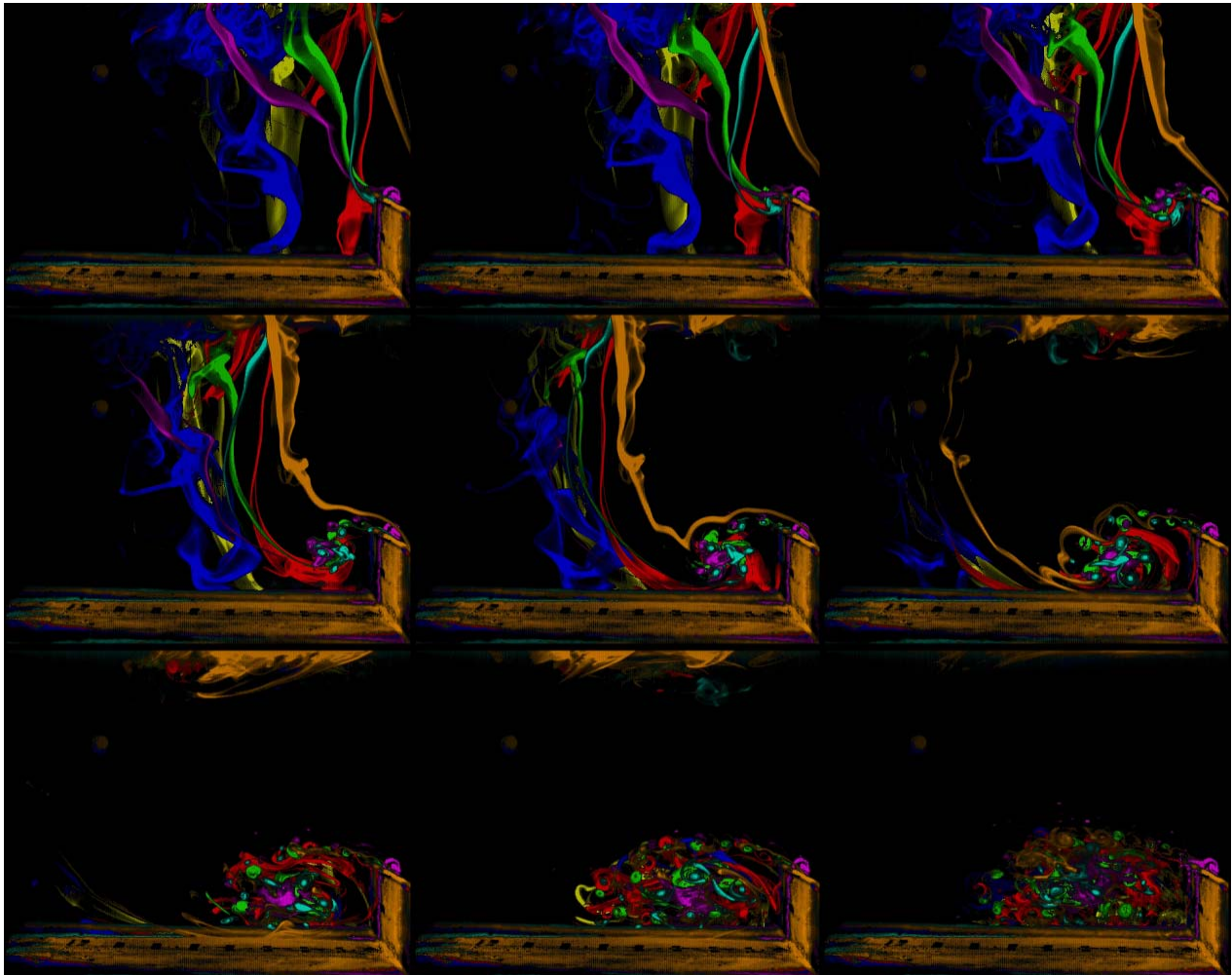


Figure 15. Superimposed Recirculation Region Growth.

After tunnel start, it can be seen in frames 1-3 of Figure 15 that the teal, purple and green immediately begin to roll up into the small vortices shown above in Figure 12. As the

recirculation region forms and develops these smaller vortices roll up into a larger vortical structure. As the recirculation region develops, downstream smoke (red, yellow and blue) begins to draw upstream as seen in frames 4 and 5 in Figure 15. Further, the orange smoke stream (originating from the upstream clutter lip) is beginning to flow over the clutter and mix into the recirculation region. However, this does not occur until the recirculation region grows to approximately 75 - 100 mm (3" - 4") downstream of the clutter. By frame 7 in Figure 15 all seven smoke streams are mixing in the recirculation region. Frames 7 - 9 show both the growth of the recirculation region from 127 mm (5.0") to 178 mm (7.0") downstream of the clutter as well as the enhanced mixing that occurs in this region.

Figure 15 clearly shows the difficulty in extinguishing a flame in the region directly downstream of the clutter since upstream air does not readily become entrained into the recirculation region that extends downstream of the clutter past the fuel pan leading edge. When the upstream smoke finally became entrained into the recirculation region, it was highly mixed with ambient air. This indicates that fire suppressant injected upstream could be heavily diluted with free stream air before reaching the recirculation region.

SUMMARY

A 2-D aircraft engine nacelle airflow simulation facility to be used for the future investigation of fire suppressant transport and pool fire extinction was presented. The facility consisted of removable elements simulating clutter in engine nacelles. Characterizations for three test section configurations were presented, one baseline (Configuration 1), and two different element configurations (2 and 3). The mean streamwise velocity was found to be 6.6 m/s (21.7 ft/s) +/- 10% for Configuration 2 and 6.3 m/s (20.7 ft/s) +/- 7% for Configuration 3. The nominal turbulent intensity was found to be 5.0 % with +/- 1% agreement across the test section for both Configurations 2 and 3. Flow visualization showed evidence that a separation and recirculation region exists directly downstream of the perpendicular clutter element. Further flow visualization showed that this region extends at least to the leading edge of the fuel pan. This supports preliminary computational results which suggest flame propagation upstream from the fuel pan to the clutter. Further, examination of the flow visualization clearly showed airflow originating downstream of the clutter being transported upstream over the clutter to a smaller upstream recirculation region. The presence of the large recirculation region and the fact that upstream airflow is not readily entrained into this region, provides some insight into the difficulty of fire protecting such a flow field found in many aircraft engine nacelles.

REFERENCES

1. Black AR, Suo-Anttila JM, Disimile PJ, Tucker JR. Numerical predictions and experimental results of air flow in a smooth quarter-scale nacelle. American Institute Aeronautics and Astronautics, Paper AIAA 2002-0856, Virginia, USA 2002, 16pp.
2. Grosshandler W, Presser C, Lowe D, Rinkinen W. Assessing halon alternatives for aircraft engine nacelle fire suppression. ASME Transaction Journal of Heat Transfer 1995;117:2.